Article:
Canzini, E., Miller, D., Tiwari, D. et al. (2026) Analysis of sensing modalities for Electrode-Induction Gas atomisation of metal powders. Surface and Coatings Technology, 525. 133276. ISSN: 0257-8972

https://doi.org/10.1016/j.surfcoat.2026.133276

Analysis of Sensing Modalities for Electrode-Induction Gas Atomisation of Metal Powders*

Ethan Canzini[a,*] (Researcher), David Miller[a] (Researcher), Divya Tiwari[a] (Project Lead), Windo Hutabarat[a] (Project Lead), Allan Matthews[b,c] (Principal Investigator) and Ashutosh Tiwari[a] (Principal Investigator)

[a]School of Mechanical, Aerospace & Civil Engineering, University of Sheffield, Mappin Street, Sheffield, S1 4DW, South Yorkshire, United Kingdom
[b]Department of Materials, University of Manchester, Engineering Building A, Oxford Road, Manchester, M13 9PL, Greater Manchester, United Kingdom
[c]Henry Royce Institute, University of Manchester, Royce Hub Building, Oxford Road, Manchester, M13 9PL, Greater Manchester, United Kingdom

ARTICLE INFO

Keywords:
Gas atomisation
In-process Sensing
Signal Processing

ABSTRACT

Electrode-Induction Gas atomisation is a crucial part of the thermal coating process, as it generates the metal powder that is used within various coating processes. A major field of analysis for powder atomisation is determining the powder yield quantity that is generated during the process. Current approaches rely on simulating the atomisation process, which fails to capture real-world physics that may interfere with the estimation of the powder yield. In this work, we outline how different sensing modalities can be used to detect the point of atomisation and how we can monitor the increasing amount of powder that is generated. Our approach covers three different kinds of sensors - contact, non-contact and visual - which can be used in parallel which each other to detect powder atomisation and collection. Using data collected from sensors attached to an Electrode-Induction Gas atomiser, we show how signal processing techniques can be used to extract information about the powder yield, thus enabling the collection of quantitative information about the powder yield. The results from analysing the signals directly link to microstructure characterisation of the generated powder which shows how sensing architectures can be used for in situ measurements of atomisation parameters. Our work demonstrates the importance of using sensors to analyse processes and demonstrates a quantitative approach to modelling the creation and yield of powder in metal atomisation, and we provide discussion topics about future directions in the field.

1. Introduction

The process of coating materials with powders remains a key part of the manufacturing cycle with applications in plasma, high velocity oxy-fuel and electric arc spraying being commonplace in surface coating applications [1]. Whilst analysing the deposition of coating process has seen increasing interest in recent years [2], one major area that influences the quality of the coated surface is the size and quality of the particles produced during the fabrication of the coating powder, which in turn affects the yield amount of powder from the production process [3], [4], [5]. Powder for coating processes is usually created through gas atomisation, a process in which molten metal is atomized through a high temperature and pressure gas [6]. Gas atomisation is a widely used method for producing metal powders, with powder yield efficiency ranging from 30-55% in conventional approaches. Through numerical modelling, previous research has demonstrated that optimising the gas nozzle design and process parameters has increased the yield of usable powder, which typically falls in the range of 15-155μm for many applications such as laser powder bed fusion [7], [8]. However, only 20-30% of the produced powder falls in the usable range and estimating the yield using numerical methods fails to capture the loss of powder that is too coarse or is filtered throughout the system. This in turn increases the time in recycling and reprocessing the powder, increasing the cost and energy use for generating the final powder yield. Whilst there have been studies on the the numerical modelling of the gas atomisation process to estimate powder yield [9], sensorization of the atomisation machine promising the best results but remains a complex task.

Many elements of in-process monitoring focus on adapting or implementing sensors onto existing machines and legacy hardware. The introduction of multiple different sensing modalities, including contact and non-contact sensors, has led to a plethora of work in adapting different sensors onto legacy hardware and processes [10], [11], thus allowing manufacturers to digitize systems that previously provided no digital information. However, a major element in digital manufacturing is the selection of sensors that provide meaningful information to the users and can be used to improve the operation of the machine so that the resulting produced product is either of a higher quality or greater quantity.

In this work, we present a multi-sensor architecture that allows for the investigation of process properties during the gas atomisation process. Our contributions are listed as follows:

1. We demonstrate that the different sensing modalities allow the capture of information during the atomisation process, both in a single atomisation and the accumulation of powder.

*Corresponding author
e.a.canzini@sheffield.ac.uk (E. Canzini)
ORCID(s): 0000-0003-1910-4267 (E. Canzini)

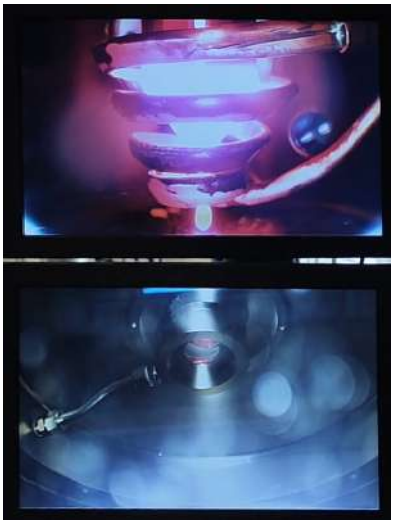

(a) Frame corresponding to the point when the metal bar melts into a droplet.

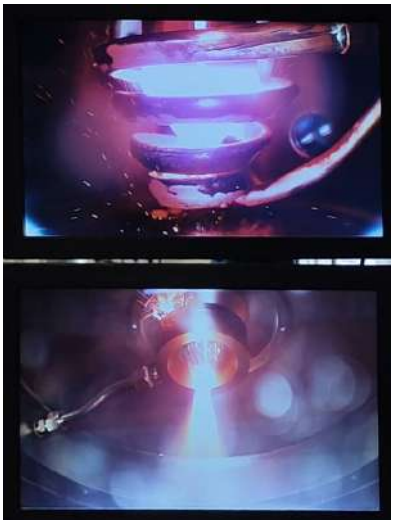

(b) Frame corresponding to the point of atomisation when the droplet interacts with the gas plume.

Figure 1: Frames from a video camera pointed at the melting coil in the upper chamber (ABOVE) and at the gas plume for the point of atomisation (BELOW). The frames correspond to when the metal has formed into a droplet (LEFT) and when the powder is created through gas atomisation (RIGHT).

2. We provide a discussion for the future of the sensorization of gas atomisation processes, including future research and industrial directions.

Our work is presented as follows: section 2 provides a literature review of the gas atomisation process, the current state of sensing on the process and the benefits of multi-sensor machine sensing. Section 3 outlines the target machine, the sensors we applied and the process parameters. Section 4 analyses the results from the experimentation, and section 5 provides a discussion about the results and how they can be used to further the research in this field.

2. Literature Review

2.1. Metal Powder atomisation

Within the scope of additive manufacturing (AM), Electrode Induction-Melting Gas atomisation (EIGA, referred to throughout this text as the atomisation process) is a key tool within the development of powder coatings. The atomisation process involves two key elements - the heating of a metal bar and the metal atomisation through contact with a high pressure and temperature gas [6]. As shown in figure 1, the metal bar is heated through a coil and creates a molten droplet, which passes through a gas inlet during which the metal atomizes and becomes a fine powder, which is deposited in the powder collector at the bottom of the machine shown in figure 1. During this process, any excess powder that is too fine to be used in coating processes is filtered out. It is for this reason that manufacturers seek to determine the powder yield from a process, as this would in turn reduce the total efficiency of the process.

Modeling the amount of powder that is collected from the atomisation process remains a complex task, as it is governed by the physical interaction of the molten metal with the high-pressure gas. The most researched method for analyzing the powder return is by modeling the interactions between the metal and the gas using finite element analysis (FEA) and computational modeling tools that can simulate these interactions [12], [13]. This can be done by assuming that the flow of the metal in free-fall is governed by the mass continuity equation:

$$\frac{\partial \rho}{\partial t} + \nabla \cdot (\rho \vec{v}) = s_m, \tag{1}$$

where ρ is the mass-flow density, $\vec{v}$ is the velocity vector of the molten metal and s_m is the mass lost to the powder that is filtered out during the atomisation process. Numerical models can be used to model both the melting of the metal bar, which governs the size of the metal droplets that interface with the gas plume, and the interaction between the metal and the gas plume [14]. These models also serve the purpose of enabling process optimization methods to be applied, such that the resulting powder yield is within acceptable bounds [9]. However, these approaches are limited by the granularity that they are simulating, which can mean the model is limited to physical effects that it can interpret. Furthermore, real-world powder atomisation physics are difficult to simulate due to the combination of the fluid flow of the metal and the particle kinetics during atomisation, meaning that simulation and numerical models cannot fully model the process.

Due to the limitations of simulation-based modeling tools, experimental validation can be used to determine the creation of powder. This can be done through the use of sensors that study specific elements of the process, such as examining the gas plume following atomisation [15]. This method can be used in combination with computational fluid dynamics (CFD) techniques to verify simulation results [16],

although this approach limits analysis to the melt plume and doesn't measure specifically the amount of powder that is retained.

2.2. In-process Sensing

In-process sensing refers to the large body of work that encompasses the inclusion of sensing apparatus in manufacturing processes. Using sensors within manufacturing allows end users and operators to discern the status of specific variables within manufacturing processes that previously could only be estimated by simulation, which enables monitoring of processes to detect and predict faults [17]. These sensors can also be used to ensure that processes don't deviate from desired parameters [18] and even to be used in the real-time control of these processes [19]. This can be further extended to aid simulation tools to model manufacturing processes using digital twins, however this requires prior knowledge of critical points in the process to ensure that all elements are being captured accurately [20].

Within surface and coatings applications, in-process sensing remains a complex task due to the large number of events and sub-processes involved. Whilst the field of coating deposition has seen increased interest in using sensors to understand the coating process [2] and has even grown to accommodate x-ray scattering as a form of real-time measurements in situ [21], the field of powder creation through gas atomisation has not seen the same success. As mentioned previously, early work focused on using high-speed imaging with Fourier analysis to monitor the melt plume [15]. The use of high-speed cinematography has also been applied with thermal imaging cameras to measure changes in droplet velocities after atomisation and use this information to build a dynamical model for the atomisation process [22]:

$$\begin{aligned} X_{t+1} &= f(X_t, U_t) \\ Y_t &= g(X_t, U_t), \end{aligned} \tag{2}$$

where X_t represents the state variables at time t, U_t is the system input, Y_t is the measurable output of the system computed from the output function g and the next state X_{t+1} is computed using the state transition function f. Computing these variables through cinematography remains an open challenge due to the computational demands of video processing algorithms. Furthermore, the main interest within gas atomisation remains to be powder quality and powder yield, the former of which is mostly determined through the use of scanning electron microscopy (SEM) methods [23]. This approach is able to quantify the amount of usable powder generated during atomisation, but can only be performed once the process is complete and thus negates the benefits of in-process sensing.

2.3. Research Gap

As we have illustrated above, using sensors to measure systems of a metal atomisation process in situ remains a key challenge, particularly for the target area of estimating powder yield. Unlike fields such as additive manufacturing or spray deposition, powder atomisation has not seen the same interest and progress for in situ sensing This has led to it being one of the parts of the deposition supply chain that lacks accurate sensing and estimation for process inspection and control. However, the issue does not arise from a lack of technological advancement - rather the gap in the literature arises from a lack of understanding as to which sensors can contribute in a meaningful way to the understanding of the process being performed. To that end, we propose an evaluation of different sensing modalities and their ability to measure the efficacy of the sensors. The use of the sensors described in this study not only mark a departure from purely vision-based sensing for powder atomisation, but also demonstrate that novel sensors that are not prevalent in machine sensing literature are able to be used in a multi-modal architecture.

3. Experimental Setup

3.1. Target Machine

To test the different sensing modalities, we target an Electrode-Induction Gas atomisation process that consists of two elements that would benefit from sensorization. The machine that was used for testing was the metal atomiser hosted by the Royce Translational Center (RTC) at the University of Sheffield. This machine consists of an upper chamber shown in figure 2a, where the metal droplet from figure 1a falls into a gas plume and atomizes. This chamber also contains two viewing ports, one of which is fitted with a light to allow for the examination of the interior of the chamber during operation. After filtering out particulates that are lost during atomisation, the powder is deposited in the lower chamber in figure 2b. This collector contains all the powder, which is then measured and sifted to determine the total amount of usable powder that was generated during the run.

From this description, it is clear to see that there are two aspects that are of interest for machine in situ sensing. The first examines the amount of powder that is generated during each atomisation pulse, and the second compares the amount of powder collected at the end of the run with the amount of metal used during the run. This would enable operators to begin to understand how process parameters such as gas temperature and pressure affect the powder yield process, and in turn help determine the mass flow model in (1). The second analyses the total amount of unusable powder that is generated from a run through the atomiser, thus allowing an estimate of the total powder generated before performing task and application specific post-process testing.

3.2. Choice of Sensors

As mentioned in section 2, the range of sensors that would be applicable to this work fall into three different categories. The first is non-contact sensors, the second is contact sensors and the third is vision systems. Each sensing modality provides unique insight to different operations that occur during the atomisation process.

(a) Atomiser Upper Chamber (b) Atomiser Lower Chamber

Figure 2: The target atomiser machine hosted at the Royce Translational Center. The upper chamber contains the gas plume that performs the atomisation of the metal droplet, and the lower chamber consists of the powder collector.

(a) (b)

(c) (d)

Figure 3: Setup of the sensors used in this study: **(a):** Acoustic-emission sensor, highlighted in red, attached to the upper chamber of the atomiser; **(b):** Vibrometer used on the upper chamber, with its laser aimed at the point of the chamber outer wall where the atomisation occurs; **(c):** The acoustic-emission sensor, highlighted in red, and the vibrometer attached to the powder collector of the lower chamber; **(d):** The event camera, pointed through a viewing port aimed at the point of atomisation.

For the contact sensor, we used an acoustic emission sensor AE WD Sensors from the Mistras Group [24]. These sensors are capable of reading inaudible high-frequency sound waves, and therefore would be able to interpret the detail from the atomisation process. Two of these sensors are mounted to the atomiser chamber - the first is mounted on the outside of the upper chamber below the point of atomisation as shown in figure 3a. The sensor was held in place using a custom designed 3D printed mount, highlighted in red, which in turn was secured to the chamber using a torque

strap shown by the green band in figure 3a. This strap applies torque to the sensor housing and ensures that there is good contact between the sensor and the chamber. The second sensor, in an identical housing and torque strap, is mounted to the lower chamber on the collector to be used for measuring the amount of powder collected. The acoustic-emission sensors were set with a sampling rate of 1.25MHz, and were connected through two pre-amps into a National Instruments Data Acquisition device (NIDAQ).

The upper chamber sensor location was chosen to focus on the vibrations generated by the molten metal impacting the gas jets. This is a major event in the manufacturing process and should be monitored closely. Additionally, there is no prior information on the volume of the impacts and how the vibrations are transmitted, therefore the sensor is placed as close as possible to provide as clean a reading as possible. The placement also does not obscure other sensors such as the camera in front of the port hole. The lower chamber location was monitored to compliment the data from the upper chamber as activity created by powder being formed in the upper chamber results in activity caused by powder being collected in the lower chamber. This acoustic emission sensor was placed after the sieves that remove gas and micro-particulates that are filtered out during operation. The locations of both the vibrometer and the acoustic-emission sensor were such that they were situated on the thinnest part of the collection chamber and therefore would be able to get the best possible readings from the collected powder dropping into the collector.

The non-contact sensor used in this study is a VibroGo OFV-5000 vibrometer sensor from Polytec [25]. This sensor operates by aiming a laser at the target surface and measuring the vibrations that occur due to changes in the wavelength of the laser through the Doppler effect [26]. As such, this makes this sensor useful for detecting changes in the vibrations of the machine, such as when the molten metal strikes the gas plume and atomises. To capture this interaction, we position a vibrometer at the top of the upper chamber where it's laser is pointed at the outer surface of the chamber level with the position at which atomisation occurs, shown in figure 3b. The vibrometer was elevated on a stand to ensure that there would be no interference with the laser. Another vibrometer was positioned at the lower chamber, shown in figure 3c, to measure the vibrations caused by the powder being deposited in the lower chamber. Both vibrometers were set to a sampling frequency of 50kHz, and were also connected to the NIDAQ system with the acoustic-emission sensors to allow for the synchronization of the time responses.

The vision system that was used during our experimentation is Prophesee Evaluation Kit 4 (EVK4), a compact system that operates over USB-C. It uses a IMX636 sensor with a resolution of 1280x720 (Height x Width, measured in pixels) that has a mounting thread making it suitable to attach onto C/CS mounts [27]. Unlike traditional cameras, event cameras operate in a similar manner to the human eye by looking for changes in the brightness of pixels to cause "events" [28]. Event cameras can detect millions of events per second, thus making them useful for detecting fast moving objects such as groups of particles caused by atomisation. To capture these particles, the event camera was situated at one of the viewing ports shown in figure 2a, where it was pointed at the space where the atomisation occurred. This setup is shown in figure 3b. To validate the findings from the event camera, the results from two cameras aimed into the upper chamber, which provide the images in figure 2, were also used as part of the vision systems software stack.

3.3. Experiment Runs

We collected data from four different runs on the atomiser. The process parameters that were changed during the runs were the gas pressure and temperature, and the parameters are detailed in table 1. The microstructure characterization was done by sorting the powder through progressively finer mesh sieves starting at the maximum useful limit of the powder of 150μm, with a breakdown for each mesh size of each run shown in table 2.

All the runs were undertaken by a trained operator who managed the flow of the metal bar, made of 316 stainless steel alloy, through the heating coil and the droplet rate through the gas plume of and the time between droplets was kept at 1s (1Hz). Run 1 was terminated early due to gas pressure loss, whereas all other runs had a total runtime of 300s. For the powder generated in these runs, the size limit for usable powder is 150μm.

Due to the number of runs and the number of sensors evaluated in this paper, we will be focusing on runs 3 and 4 in our specific analysis. However, all the runs have been evaluated, with their plots alongside the code to generate the plots and analysis written in Python and MATLAB available on our GitHub repository here. We provide the raw collected sensor data in TDMS format here [29]. Note that given the size of several of the datasets, it is recommended to use a High Performance Computer (HPC) that has access to large amounts of RAM to ensure that the dataset can be loaded correctly.

4. Methodology & Analysis

4.1. Vibrometer Analysis

The vibrometer sensor collects readings based on the vibrations that occur within the chamber. As the upper chamber is water-cooled, this causes a background noise floor in vibrations during operation. This can be seen in figure 4a, where there is a high degree of noise in the readings. However, the underlying waveform that corresponds to the readings from the sensor is visible in the latent frequencies, highlighted in red in figure 4a. As such, filtering out this noise would illustrate the signal that is hidden within the noise.

Choosing the frequencies that are relevant and those that are to be filtered out requires avoiding the time domain response and looking at the frequency response of the waveform. Wavelet analysis [30] alleviates the uncertainty principle associated with Fourier transformations by exploiting multi-resolution decomposition. Using the continuous

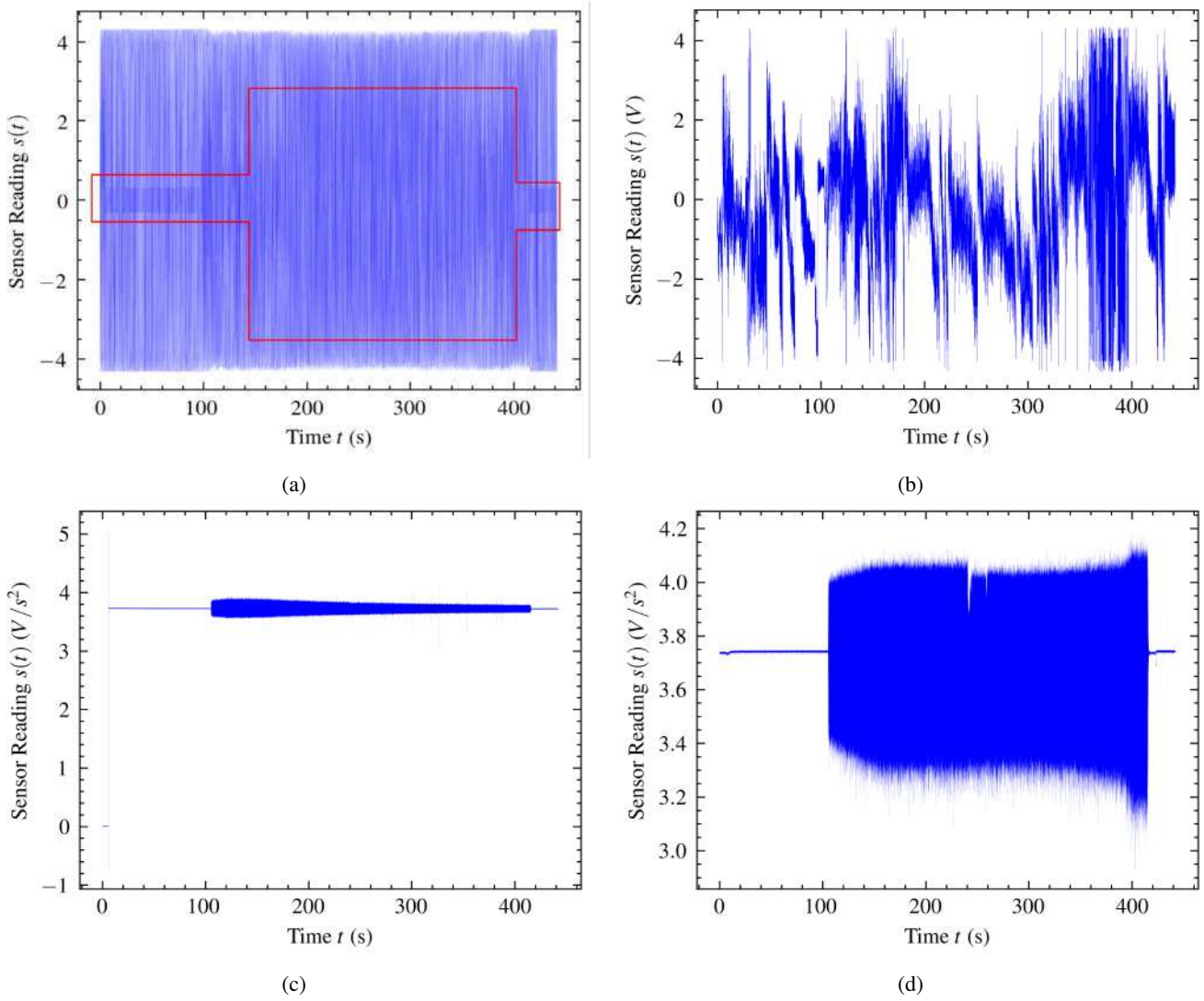

Figure 4: Time series plots of the results from the vibrometers and acoustic-emission sensors, taken from run 4. The top row corresponds to the vibrometer readings, with the red box highlighting the underlying frequencies in **(a)**. The bottom row corresponds to the acoustic emission sensor readings. The left column corresponds to the upper chamber, whilst the right column is the lower chamber. Further plots for the other runs can be found in Supplementary Material A.

Table 1
Table of process parameters used across the four runs of the atomiser.

Run	Gas Pressure (bar)	Gas Temperature (°C)	Mass of Produced Powder (kg)
1	50	100	2.351
2	70	100	1.529
3	70	300	1.584
4	50	300	1.616

Table 2
Table of microstructure characterization of the powder from all four runs, given as a percentage of the total powder generated when sorted by sieve mesh sizes.

Run	$<45\mu$m	45-53μm	53-63μm	63-75μm	75-106μm	106-120μm	120-150μm	$>150\mu$m
1	7%	2%	2%	9%	28%	9%	10%	32%
2	15%	4%	4%	8%	19%	11%	9%	30%
3	11%	3%	2%	6%	13%	10%	7%	48%
4	15%	4%	3%	7%	18%	10%	9%	33%

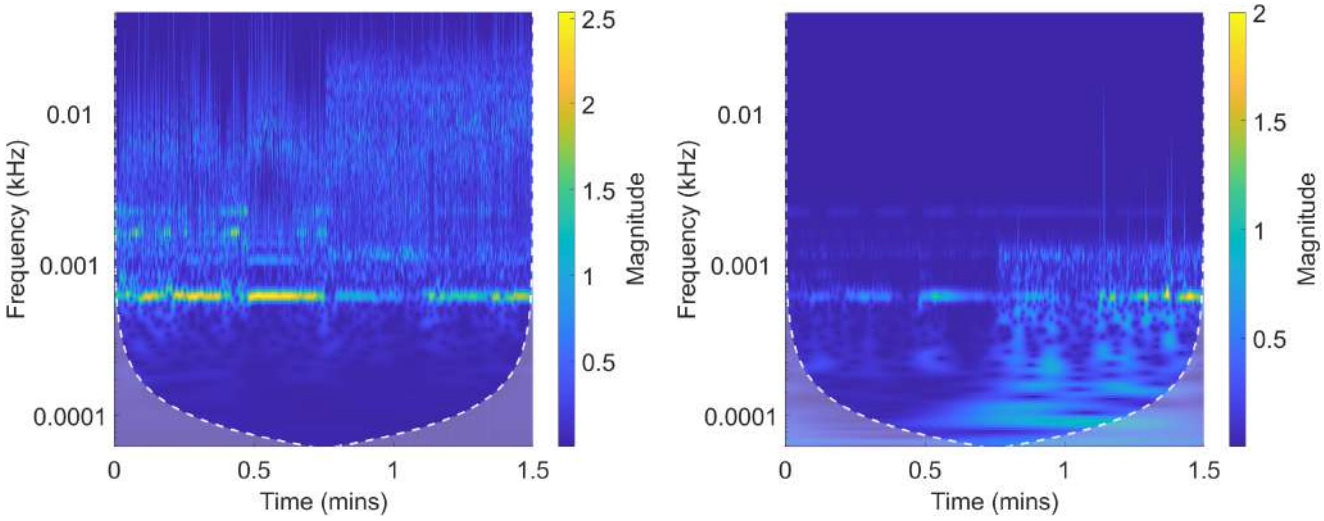

(a) Run 3 - upper chamber

(b) Run 3 - lower chamber

Figure 5: Continuous wavelet transforms for the upper (LEFT) and lower (RIGHT) chamber vibrometers. The complete set for all CWT plots for all runs can be found in Supplementary Material B - CWT Plots.

wavelet transform (CWT), we can analyse a signal in the time and frequency domains using the Morlet wavelet:

$$\psi(t) = \frac{1}{\sqrt{\pi B}} \exp\left[2i\pi f t\right] \exp\left[\frac{-t^2}{2\sigma^2}\right], \tag{3}$$

where f is the centre frequency in Hz, t is the time in seconds, B is the bandwidth parameter and σ is the width of the Gaussian window defined by the number of cycles constant n:

$$\sigma = \frac{n}{2\pi f}. \tag{4}$$

The Morlet wavelet was chosen as the responses we are looking for in the atomisation process are periodic which the Morlet is designed to search for within the signal. The oscillatory shape of this wavelet makes it useful for identifying signals of high frequencies and the complex nature captures both the magnitude and phase information of the signal. As the phase information requires far more computational resources and yielded little tangible results in our testing, we focus on the magnitude of the wavelet analysis.

The CWT analysis was performed by examining the time when the atomisation process was initiated after the machine had been left running to ensure that an adequate noise floor could be established. At the atomisation start time, 30s of operation were recorded either side of the start time, as CWT analysis looks at changes in the frequencies and would require information regarding the time with no atomisation to allow for a frequency comparison to the time period of atomisation. Figure 5 shows the CWT analysis for the upper and lower chamber vibrometers. As shown in figure 5a, there is a periodicity at 1Hz that aligns with the droplet speed, indicating that the upper vibrometer is able to detect the moment of atomisation. As each pulse has a different magnitude, this means that the vibrometer is detecting different sized pulses based on the size of the droplets as their interact with the gas plume. The spiking frequencies in the plots are evidence that the powder atomisation process is not uniform, hence reinforcing the mass-continuity information as different powder sizes would cause different vibration frequencies. As such, the frequencies correspond to the different particle sizes as they cause different vibration magnitudes.

Looking at figure 5b, the lower vibrometer also detects the 1Hz droplet rate initiated by the operator. However, the lower vibrometer also detects different frequencies that align with the powder being deposited in the lower chamber. These frequencies, similar to the upper chamber, are at different magnitudes which indicates that this represents different amounts of powder being deposited in the collector. By comparing the magnitudes at similar times on the CWT analysis, such as those in figure 5a, we see that the magnitude of spikes is less in the lower chamber compared to the upper chamber, showing us that the magnitude of powder atomisation correlates to the powder size whereas the lower chamber is able to estimate the loss of the powder due to atomisation.

Another interesting analysis of the lower chamber vibrometer is that there is an underlying low frequency that perpetuates through the signal. Unlike the high frequency noise, this signal is of a higher magnitude and fluctuates across the time domain. These frequencies are generated due to the size of the powder that is collected in the lower chamber that does not satisfy the usable particle size for coating applications. As the different sizes of the particles would cause different vibrations in the lower chamber, cataloguing these pulses and comparing them against the amount of useful powder collected would allow the identification of the vibrational response of the powder that is the desired size.

4.2. Acoustic-Emission Sensor Analysis

Examining the responses of the acoustic-emission sensors in figure 4, the first observation to be made is that the upper chamber vibrometer is useful for detecting the exact start of the atomisation process. In figure 4c, the sensor reading changes the moment atomisation occurs, but only registers a consistent waveform for the duration of the process. This indicates that the atomisation process does not involve frequencies in the megahertz range. The lack of high frequency components in the upper chamber, which can be verified by examining the frequency components in figure 5a, informs us that the interaction of the metal with the gas plume, and the subsequent atomisation, is only present in low frequencies. This was further illustrated in the previous section when discussing the vibrometer analysis, in particular the frequency responses in figure 5. However, the magnitude of the signal across runs 3 and 4 varies, where both runs were kept at a gas temperature of 300°C but changed the gas pressure from 70 bar to 50 bar. Therefore, whilst specific pulses and points of atomisation cannot be detected, the upper chamber acoustic-emission sensor can be used to validate both the runtime and the gas pressure of the chamber based on the magnitude and length of the sensor readings.

Moving onto the lower chamber acoustic-emission sensor, this response is very different to its predecessor. There is an increasing amplitude in the sensor readings as the time for atomisation increase, which is also mirrored in the lower half of the sensor reading. This mirror in the sensor reading is due to the "rattling" of the lower chamber as powder is deposited, with the changing amplitude corresponding to the changing modal frequencies of the chamber as the amount of powder deposited in the collector increases. Whilst the knowledge of these frequencies is useful for computing the amount of powder in each moment of atomisation, as described in section 4.1, the results from the acoustic-emission sensor show a cumulative distribution of how the powder is collected, indicating that the amount of powder that is above the usable maximum particle size of 150μm is detectable.

To model the cumulative distribution of powder using the acoustic-emission output, we examine the energy of the signal across the time of atomisation. Signal energy, whilst synonymous with the physics interpretation of energy, examines the size of the square of a signal and can be explained as the measure of the strength of a signal with both real and imaginary parts [31]. For discrete time signals, the energy is defined as the dot product for each sample n in a time-domain response, which in equal to the sum of squares of a signal between two bounds N_1 and N_2:

$$\begin{aligned} E[n] &= \langle x[n], x[n] \rangle \\ &= \sum_{n=N_1}^{N_2} |x[n]|^2. \end{aligned} \tag{5}$$

This calculation can be very susceptible to noise, and thus would amplify low-frequency components in the acoustic-emission response which would cause undesirable readings.

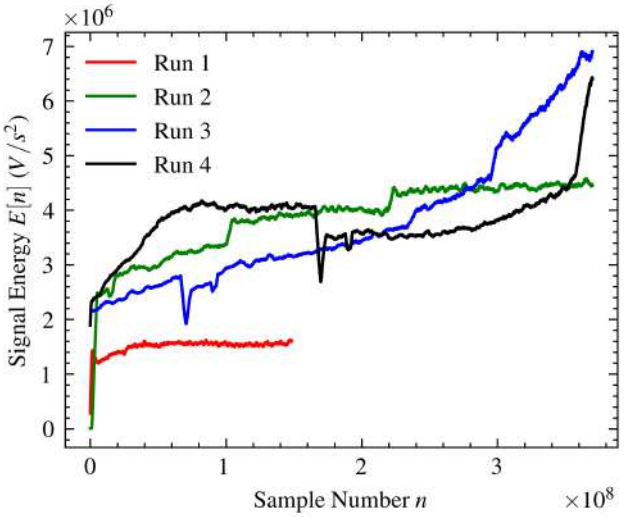

Figure 6: Plots of the signal energy for the four runs on the atomiser.

As such, the energy function calculation in (5) can be modelled as a convolution operation to mitigate the effect of spectral leakage has on the energy calculation. Additionally, the window function enables the bounding of the energy calculation to the region of the time-domain response where the atomisation process is taking place. Let $X[n]$ be the energy function described in (5). The convolutional energy is defined as:

$$\begin{aligned} E[n] &= (X * W)[n] \\ &= \sum_{m=0}^{M} |x[m]|^2 \, w[n-m], \end{aligned} \tag{6}$$

where $W[n]$ is the window function used in the operation. For our calculation, we used Hamming window function across the sample range $0 \leq n \leq N-1$ defined as:

$$w[n] = a_0 + (1 - a_0) \cos\left(\frac{2\pi n}{N}\right), \tag{7}$$

with $a_0 = 0.54$ and N being the number of samples in the size of the window. As our sensor reading is measured in Volts V, the units for the signal energy are V^2/s. As the time between droplets is 1 second but there is considerable settling in between droplets, we set N to be 1.25×10^6 in line with the sampling frequency of the acoustic emission sensor in section 3.2 to better capture the data of the powder settling in the lower chamber.

Figure 6 shows the energy plots for each run from the start of the atomisation process until the process ends. Despite run 1 being terminated early on the advice of the operator, all four runs show different energy responses over the atomisation process and a different final energy result. We can see that the lower chamber acoustic-emission sensor is able to detect the amount of powder outside of the usable range generated by using the energy of the signal. Furthermore, we can also compare the lower chamber vibrometer reading with that of the acoustic-emission sensor to evaluate

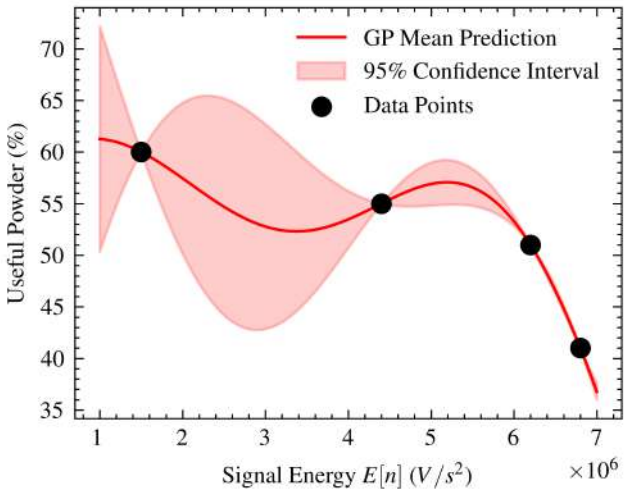

Figure 7: Plot of the resulting GP regression model comparing the signal energy $E[n]$ against the percentage of usable powder generated.

the performance of the atomisation process. Generating consistent amounts of powder during each interaction between the molten droplet and the gas plume is important to ensure that the quality of the powder is maintained throughout the process. Looking at figure 6, we see that run 3 showcases the most consistent and smooth energy response for the cumulative amount of powder, which is mirrored by the response in figure 4b where the frequency magnitude response in the lower chamber vibrometer shows a repeated pattern of powder being collected in the lower chamber, therefore showcasing that run 3 generated the most powder that was above the usable range.

A further point of analysis that can be developed is the creation of a regression model to predict the percentage of usable powder given a total signal energy. Such a model would be able to provide insight to how different energy signals - and thus machine parameters - affect the production of useful powder. For this analysis, the amount of useful powder is determined by looking at powder that is within the useful ranges in table 2. The regression model used for this analysis is a Gaussian Process (GP) with a Radian Basis Function (RBF) kernel, chosen for its ability to provide both reliable estimations from small datasets and uncertainty bounds in regions with little to no data [32]. The resulting plot in figure 7 further demonstrates the relationship between the signal energy and usable powder generated, indicating that a higher signal energy, which corresponds to larger particles being generated, leads to lower usable powder.

4.3. Event Camera Analysis

The majority of ways to process event data is to accumulate event packets over a fixed time period, known as accumulation time, and apply some function. One of the simplest is counting the number of events. As the event camera only generates data in response to changes in light, the number of events in a given time period is a reliable indicator of activity. In these experiments, the main event of interest is the molten metal impacting the gas jet. This creates a large and intense burst of light, which should generate a large number of events with positive polarity.

Figure 8a shows an example of this. This frame was generated by setting the accumulation time to 14825 μs. This value was derived from reviewing the footage and finding a value that offered the clearest view of potential objects of interest whilst minimising background noise. The non-black pixels indicate locations with at least one event with positive polarity. The density of the events increases to a peak before decreasing and disappearing over an estimated period of approximately 0.06 s from the timestamps. Afterwards there are very few events, suggesting that the brightness is consistent making it difficult to perceive changes. On some occasions, streaking particles were observed travelling from the bottom of the frame to the top.

Plotting the number of events using an accumulation time of 2ms produces a very dense signal that is difficult to see even if it is filtered to only events with positive polarity only. Figure 9 shows the number of events over time for Run 3 including graphs for only positive and negative events. There is a maximum of 10000 events due to setting a maximum event rate to avoid encoding errors observed in Run 1. The start and end of the run are clear from sudden increases in the signal, but the flashes of interest are hidden.

Figure 10 shows the results of the CWT applied to the number of positive events for Run 3 and Run 4. The data along the Y-axis are generated by applying a scaling factor to the wavelet function which stretches it enabling the capture of behaviour at different frequencies. The X-axis represents time in microseconds, the Y-axis represents frequency in Hertz (Hz), and the magnitude is the response to the scaled wavelet function. This approach reveals a clear component that is active for the duration of the atomisation process. For both Run 3 and Run 4, this component stays fairly consistently at 1 Hz suggesting this is the rate the droplets are being atomised. The vertical lines stretching from lower to higher frequencies are transient events that occur over a very narrow time period.

These results can be validated by checking the video footage used to make Figure 1. This footage was taken using a Nothing 1 phone at 1920 x 1080p at 60 fps. Whilst the data gathered through this medium can be used for verifying the event camera data, using a phone camera within our multi-modal sensor system is a low-fidelity check which can be improved through the use of high speed video cameras. The phone was pointed towards two displays showing the footage from two cameras looking into the atomiser. One camera is pointed towards the coil where the metal bar is rotated at a fixed speed and heated until globs of molten metal fall (Figure 1a). The other camera is pointed upward at the nozzle where the powder hits the gas jet (Figure 1b). When molten metal hits the gas jet, it causes a bright flash of pixels. As the phone was physically held as opposed to being held on a stand, the field of view (FOV) moves around and occasionally points away from the screen. A simple

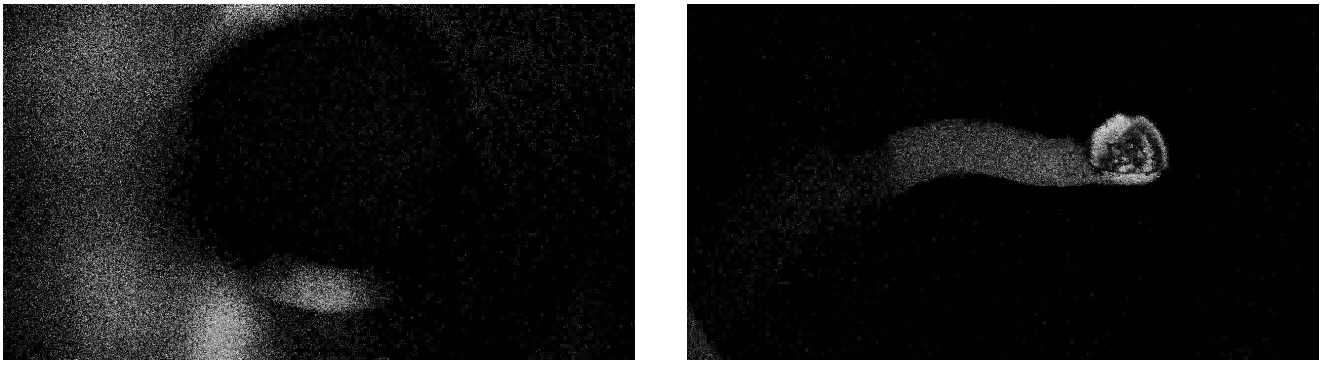

(a) Example of the powder impacting the gas stream.

(b) Example of observed objects moving across the frame

Figure 8: Frames taken from the event camera by setting the accumulation time to 14825μs at 500 FPS.

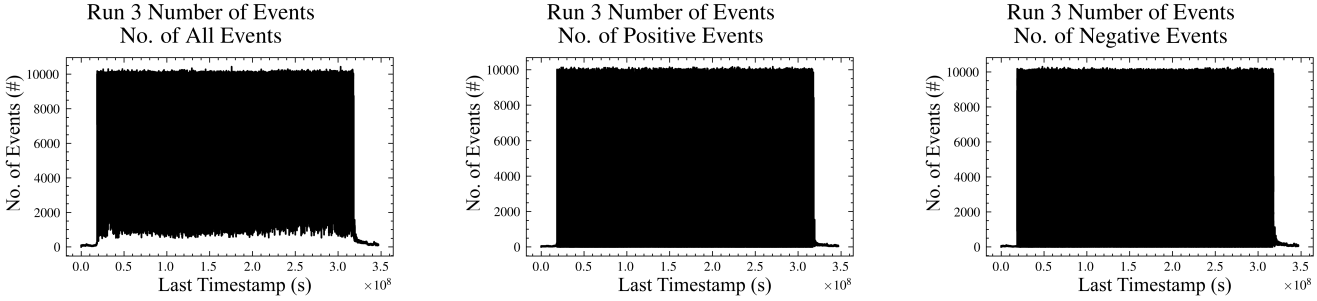

(a) All Events

(b) Positive Events

(c) Negative Events

Figure 9: Number of events in Run 3 using an accumulation time of 2000 μs

algorithm was developed to isolate the displays and then track the number of bright pixels. First, pixels in the colour range 0-50 are identified and used to create a binary image. The largest contour surrounding these pixels is believed to be the two monitors. The image is cropped to this to remove extraneous objects. Finally, bright pixels are identified by searching for pixels in the colour range 180-255. These ranges were identified through manual adjustment. This algorithm is summarized in Figure 11.

The flash caused by the molten metal hitting the gas causes a brief peak in the number of pixels. To identify the peaks, the *find_peaks* function part of Scipy [33] is used. The minimum distance and prominence parameters were tuned to try and eliminate unwanted peaks. The results of Run 3 and Run 4 are shown in Figure 12. The plot was clipped to a specific period to avoid the times when the camera was not pointed at the monitors.

The distance between neighbouring peaks can be used to estimate the frequency of the flashes. The distances are

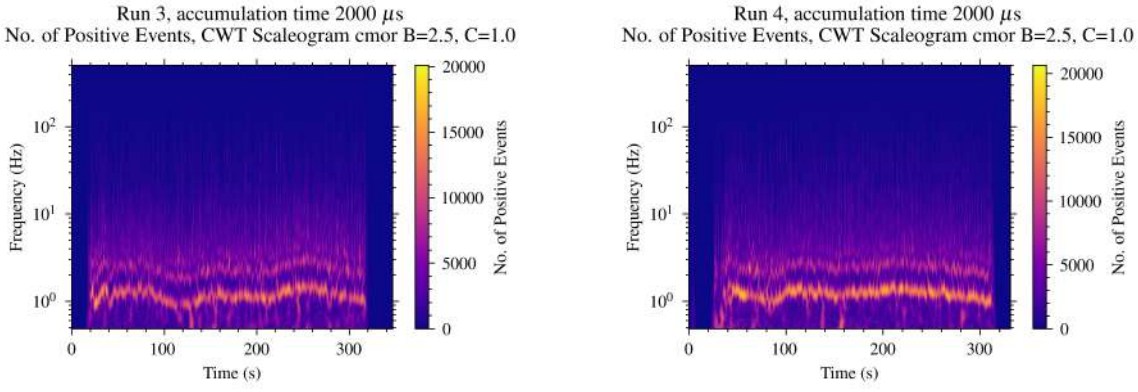

(a) Run 3

(b) Run 4

Figure 10: CWT of the Number of Positive Events collected with an accumulation time 2000μs using cmor2.5-1.0

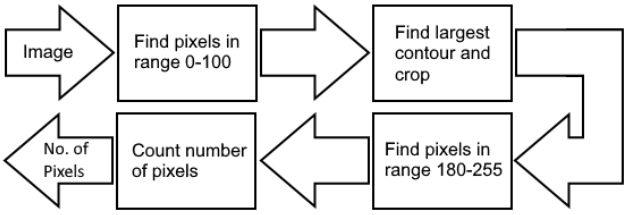

Figure 11: Algorithm used to isolate bright pixels in mobile footage

converted from samples to seconds by dividing by the video frame rate. The resulting data is filtered by removing any values further than two standard deviations from the mean. This is to remove outliers that are clearly not part of the main trend. Taking the average of the filtered data and finding the inverse provides the frequency in Hertz (Hz). Figure 13 shows the peak distances in seconds after filtering. Figure 13a shows an average of 1.13 Hz, and Figure 13b shows an average of 1.30 Hz. This is in the same frequency range identified in the CWT of positive events in Figure 10.

An established value of event cameras is the ability to track and record the motion of objects [34], [35], [36]. In a powder atomiser, the movement of molten particles and how their shape changes is of key interest as the amount of powder that forms in the powder collecting chamber is a core performance metric. To capture the motion as an image, the event camera data was encoded as a time surface. This approach accumulates event data over time creating an image where each pixel has a value representing the cumulative activity of that area where higher values corresponds to more recent movement [28]. The method used normalizes the time surface so the last timestamp has a value of 255 and the last timestamp minus a delta value, set to 500 microseconds, is set to 0. An accumulation time of 14285 microseconds was chosen based inspecting the data and noting how long major events lasted.

Several interesting behaviours can be observed in this data. Figure 14 show sets of sequential frames organised left to right from the time surfaces for Run 2,3 and 4. The frames show a distinct object moving across the frame. The size of the object relative to the frame size suggests that the event camera was out of focus. It should be noted that it was difficult to focus the event camera in these circumstances as the particles would be occurring at various distances from the camera so some portion would always be out of focus. Additionally it would be difficult to insert an object into the chamber to act as a reference point. Additionally, focusing event cameras so that the events are in focus at all times remains an open problem within computer vision applications. As it cannot be confirmed if these objects are one or several droplets, they will be referred to as objects. This is reinforced by how few objects there are. From viewing the mobile phone footage, the molten droplets clearly split into many smaller droplets rather than the few seen. However in the time surface, there is generally a maximum of 5-7 objects on screen. Figure 14a shows an example of when the objects begin travelling in a circular pattern before disappearing. Opposite the camera behind these objects is a pipe that is designed to extract unwanted particles and prevent them from entering the compressor. The diameter of the path made aligns with the diameter of that pipe suggesting this is tracking one or several powder particles being drawn into the pipe. The head of the object visually has the higher value meaning over the accumulation period has the most motion. Figure 14b shows the moment when the path first enters this behaviour.

Figure 14c is an example of when multiple objects are travelling through the frame. In addition to the force provided by the pipe on the other side, the objects are being pulled upwards back to the gas jet at the top by a vacuum force created by gas turbulence flows. Many of the objects observed across all runs were observed travelling vertically with some captured turning around falling towards the chamber.

5. Discussion

The results in the preceding section highlight three different sensing modalities and their efficacy of detecting elements of the powder atomisation process. All three sensors capture different parts of the atomisation process, which together provide a clear image of the atomisation process. By using the non-contact vibrometer on the upper chamber, the atomisation droplet rate of 1Hz can be independently verified which enables powder producers to develop system verification tools and provide their consumers with evidence of the process parameters. When the vibrometer is used to detect powder deposition in the lower chamber, the time-frequency response can be used to examine the amount of powder that is deposited in the collector after each atomisation. As both of the vibrometers have latent responses at 1Hz, one can examine the magnitude peaks at the corresponding times to provide an estimate of the powder loss at each atomisation instance, which can be used to evaluate the mass continuity from (1). This in turn can be used for data-driven approaches to generate labels and data-points for learning the mass continuity of the at different process parameters [37].

Our choice of contact sensors, the acoustic-emission sensors, were limited to providing information regarding the runtime of the atomisation process and verifying the gas pressure used in the run due to the lack of high frequency components in the upper chamber of the atomiser. This information is useful for determining the powder to time ratio, examining the efficiency of the process for given droplet rates. On the lower chamber, the acoustic-emission sensor readings are able to read the increasing amount of cumulative powder that is collected which is above the usable size of 150μm. This result is one of the most pressing for the production of coating powders, as this can be used to dictate the percentage efficiency of the powder atomisation process and which process parameters provide the best ratio of produced powder. This is shown by comparing the results in figure 6 with the final column in table 2, which shows

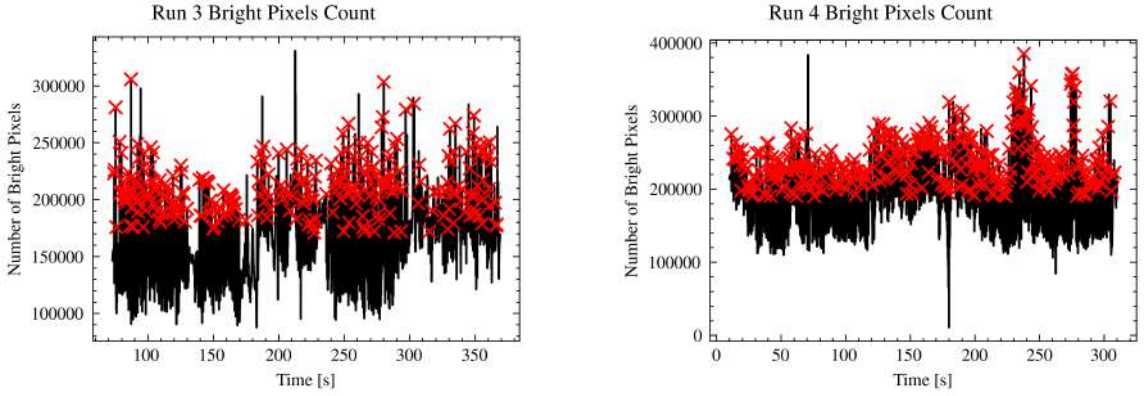

(a) (b)

Figure 12: Number of bright pixels identified in the mobile footage for Run 3 (a) and Run 4 (b)

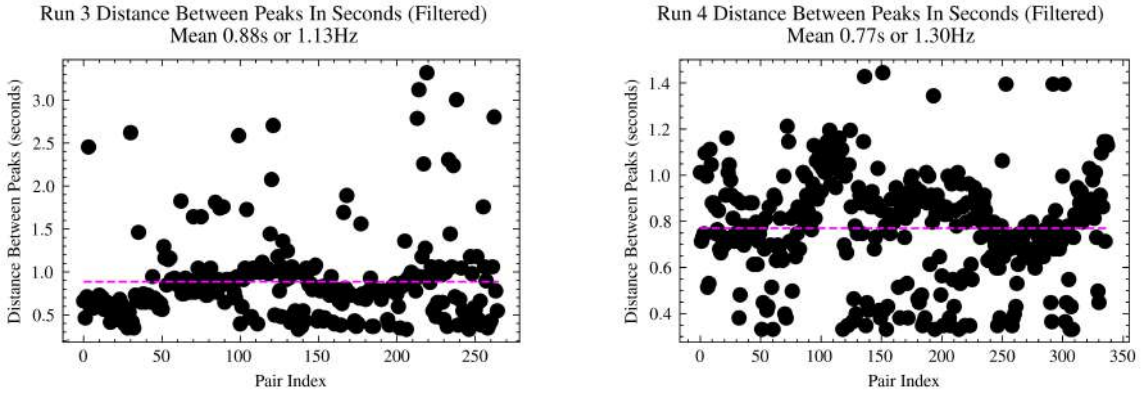

(a) (b)

Figure 13: Distance in seconds between peaks of bright pixel counts after filtering for Run 1 (a) and Run 2 (b)

that run 3 had the highest amount of unusable powder and the highest energy. This happens because the larger particle sizes cause the most vibrations when they are deposited in the collector, hence increasing the signal energy. By combining this information with the readings from the lower chamber vibrometer, the amount of powder generated in each atomisation interaction can be combined with the increasing amount of powder in the collector to determine which powder sizes are detectable and thus quantify the amount of useful powder generated during each atomisation run.

The vision system of the combined event camera and mobile phone camera allows for the verification of particle droplet sizes after the atomisation event. By examining the magnitude of the events detected by the event camera, the size of clumps of particles can be estimated and this helps with the determination of the amount of powder generated during each atomisation event. Additionally, this can be useful for examining how particles clump together after atomisation which in turn can be linked to the quality of powder that is generated. Another benefit of the event camera results are the further verification of the time between pulses that is generated by the operator.

One limitation of the sensors we have presented in this work is, whilst we are able to quantify the amount of unusable powder from the process, we cannot provide estimations of the specific types of usable powder, as shown in the breakdown in table 2. This is due to the fact that the shapes and sizes of the individual powder can only be determined through the use of powder sieves or SEM images [23]. One possible way to quantify the specific sizes of powder related to sensor readings in situ would be to measure a single droplet through the sensors, then evaluate the SEM and powder sieve results from this droplet. However, given the cost of doing single droplet runs to characterise each size of particle and that different size particles are used for different applications in coating technologies, it would be more beneficial and cost effective to utilise the in situ measurements to determine the amount of unusable powder generated from the process, then use post-processing techniques to determine the amount of usable powder generated for specific applications.

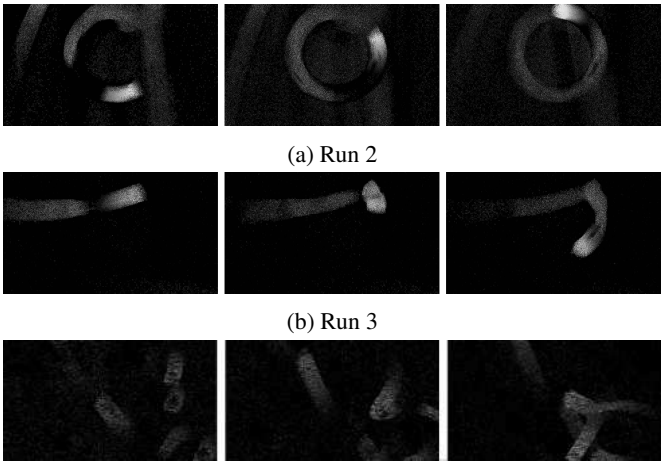

(a) Run 2

(b) Run 3

(c) Run 4

Figure 14: Three sequential time surface frames organised left-to-right calculated using an accumulation time of 14285 microseconds for Run 3 (a) and Run (4)

From these results, it is evident that in situ sensing has the potential to enhance the capabilities of metal atomisation by providing feedback on the amount of powder that is above the usable size. To take this work further, there are several avenues within sensing and signal processing that would provide the most benefit. Firstly, by performing single droplet analysis and measuring the amount of powder generated in each drop, the magnitudes of individual atomisation events could be quantified in the wavelet plots in figure 5. This in turn would enable the classification of different particle sizes based on their respective frequency bands, which would allow a greater understanding of the distribution of particle sizes whilst the machine is operational. Additionally, the wavelet responses could be analysed further to generate noise frequencies that could be filtered out through the design of filters. Of particular note for this application would be a high pass filter than attenuates low frequencies that would be caused by background noise. However, both of these approaches raise an important point regarding the time and material spent on running specific tests for determining droplet and particle sizes. Simulation tools can bridge the data gap in terms of process parameters [9], [14], but inaccurate sensing and disturbance models would limit the efficacy of the simulated data when compared against experimental results. Another approach would be to leverage methods in Generative Artificial Intelligence (GenAI) to create simulated datasets based on knowledge of system physics and prior datasets. However, this poses a new set of concerns, namely regarding the consistency of the data and the hallucination characteristics of GenAI models that cause them to “imagine" data points [38], [39]. As such, for metal atomisation processes the collection of experimental data remains the only viable solution to determining output parameters.

For the vision systems, the results in this paper demonstrate that event cameras can be used for finding out the size of clumps of particles during atomisation. The next step with this sensor would be integration with other vision systems such as thermal and RGB cameras. This would allow the tracking of particles during atomisation, and would also allow precise estimation of the size and temperature of the particle clumps, which in turn would provide information about the quality of the particles. One of the biggest technical limitations of this sensor setup is the difficulty in focusing the event camera. Adding extra cameras, positioned at different angles could help inform where to focus the camera. The powder atomiser has multiple port holes directed into the chamber for monitoring. The event camera used in the experiments was positioned to capture the vertical velocity of objects. Another camera positioned at one of the other port holes could capture the breadth of the particle spread and show where the greatest concentration of particles is. A reference object can then be inserted into the chamber at the target depth. This would have to be performed before pulling a vacuum inside the chamber, greatly increasing operation time. The objects themselves could also be classified through this approach, which could be paired with other vision systems to categorise the objects based on particle sizes and whether the powder has formed a mass. Additionally, both the vision system and the sensors could be integrated into the controller of the atomiser itself to enable optimisation of the process parameters to improve the overall powder yield, thus providing real-time feedback about the quantity of usable powder during operation. During the experiments, the droplet rate of material was manually tuned by a trained technician. With the demonstrated ability to monitor it, a control loop can be constructed that provides corrections either directly to the controller or suggestions to the technicians.

6. Conclusions

In this paper, we present a novel approach to monitoring the metal atomisation process. Our work represents the first approach in literature to provide a quantitative analysis and modelling of the powder creation and yield by combining three different sensing modalities - contact, non-contact and vision - to demonstrate that important characteristics of the atomisation process related to powder yield can be captured. By using these sensors, direct measurements can be made on the nature of the powder yield within the usable band. The sensors are deployed on a metal atomiser with different process parameters to show that the chosen sensors are not limited to single processes. We provide analysis results of the three modalities, along with discussion topics for future work.

CRediT authorship contribution statement

Ethan Canzini: Conceptualization of this study, Methodology, Results Analysis (Vibrometer and Acoustic-Emission Sensors). **David Miller:** Conceptualization of this study, Methodology, Results Analysis (Event Cameras). **Divya**

Tiwari: Conceptualization of this study, Project management. **Windo Hutabarat:** Conceptualization of this study, Project management. **Allan Matthews:** Project management & supervision. **Ashutosh Tiwari:** Project management & supervision.

Acknowledgments

The authors would like to acknowledge the support of Dr. Robert Deffley and the team at the Royce Institute at the University of Sheffield for providing access to the gas atomiser used in this study to collect results, and for providing technical insights into the working processes of the system.

The authors would like to acknowledge Dr. Robin Mills at the Laboratory for Verification & Validation (LVV) at the University of Sheffield for the rental of the vibrometer sensors used in the experiments.

References

[1] A. S. Dinkar and H. Panchal, "A review on thermal spray coating processes," en, *International Journal of Current Trends in Engineering & Research*, vol. 2, no. 4, pp. 556–563, 2016.

[2] D. Miller, V. Viswanathan, D. Tiwari, W. Hutabarat, S. Goel, B. M. Irungu, A. Matthews, and A. Tiwari, "Monitoring of Argon plasma in a coating manufacturing process by utilising IR imaging techniques," *Journal of Manufacturing Processes*, vol. 138, pp. 79–89, Mar. 2025, ISSN: 1526-6125. DOI: 10.1016/j.jmapro.2025.01.093.

[3] H. Yin, H. Too, and G. Chow, "The effects of particle size and surface coating on the cytotoxicity of nickel ferrite," en, *Biomaterials*, vol. 26, no. 29, pp. 5818–5826, Oct. 2005, ISSN: 01429612. DOI: 10.1016/j.biomaterials.2005.02.036.

[4] G. Bae, K. Kang, H. Na, J.-J. Kim, and C. Lee, "Effect of particle size on the microstructure and properties of kinetic sprayed nickel coatings," *Surface and Coatings Technology*, vol. 204, no. 20, pp. 3326–3335, Jul. 2010, ISSN: 0257-8972. DOI: 10.1016/j.surfcoat.2010.03.046.

[5] S. Sarangi, J. A. Weibel, and S. V. Garimella, "Effect of particle size on surface-coating enhancement of pool boiling heat transfer," en, *International Journal of Heat and Mass Transfer*, vol. 81, pp. 103–113, Feb. 2015, ISSN: 00179310. DOI: 10.1016/j.ijheatmasstransfer.2014.09.052.

[6] I. Chang and Y. Zhao, Eds., *Advances in Powder Metallurgy: Properties, Processing and Applications* (Woodhead Publishing Series in Metals and Surface Engineering). Chantilly, United Kingdom: Elsevier Science & Technology, 2013, ISBN: 978-0-85709-890-0.

[7] S. Özbilen, A. Ünal, and T. Sheppard, "Influence of Liquid Metal Properties on Particle Size of Inert Gas Atomised Powders," *Powder Metallurgy*, vol. 39, no. 1, pp. 44–52, Jan. 1996, ISSN: 0032-5899. DOI: 10.1179/pom.1996.39.1.44.

[8] S. Mandal, A. Sadeghianjahromi, and C.-C. Wang, "Experimental and numerical investigations on molten metal atomization techniques – A critical review," *Advanced Powder Technology*, vol. 33, no. 11, p. 103 809, Nov. 2022, ISSN: 0921-8831. DOI: 10.1016/j.apt.2022.103809.

[9] S. Spitans, H. Franz, and E. Baake, "Numerical Modeling and Optimization of Electrode Induction Melting for Inert Gas Atomization (EIGA)," en, *Metallurgical and Materials Transactions B*, vol. 51, no. 5, pp. 1918–1927, Oct. 2020, ISSN: 1543-1916. DOI: 10.1007/s11663-020-01934-5.

[10] E. Canzini, M. Auledas, D. Chasteau, and A. Tiwari, "A Novel Sensing Template Utilising Data Fusion for Large Volume Assembly," in *14th IFAC Workshop on Intelligent Manufacturing Systems*, ser. IFAC-PapersOnLine, vol. 55, Tel Aviv-Yafo, Israel: Elsevier Ltd, 2022, pp. 283–288. DOI: 10.1016/j.ifacol.2022.04.207.

[11] D. Miller, B. Song, M. Farnsworth, D. Tiwari, F. Freeman, I. Todd, and A. Tiwari, "IoT and Machine learning for in-situ process control using Laser Based Additive Manufacturing (LBAM) case study," *Procedia CIRP*, 54th CIRP CMS 2021 - Towards Digitalized Manufacturing 4.0, vol. 104, pp. 1813–1818, Jan. 2021, ISSN: 2212-8271. DOI: 10.1016/j.procir.2021.11.306.

[12] J. Wu, M. Xia, S. Guo, J. Wang, and C. Ge, "Effect of electrode induction melting gas atomization process on fine powder yields: Diameter of free-fall gas atomizer," en, *Journal of Materials Engineering and Performance*, vol. 32, no. 8, pp. 3390–3400, Apr. 2023, ISSN: 1544-1024. DOI: 10.1007/s11665-022-07366-3.

[13] C. Ge, M. Xia, J. Wu, and J. Wang, "Effect of electrode induction melting gas atomization process on fine powder yields: Continuous metal melt flow," *Archives of Metallurgy and Materials*, vol. 68, no. 3, pp. 839–840, Sep. 2023, ISSN: 2300-1909. DOI: 10.24425/amm.2023.145446.

[14] V. Bojarevics, A. Roy, and K. Pericleous, "Numerical model of electrode induction melting for gas atomization," *COMPEL - The international journal for computation and mathematics in electrical and electronic engineering*, vol. 30, no. 5, F. Dughiero, E. Baake, and M. Forzan, Eds., pp. 1455–1466, Jan. 2011, ISSN: 0332-1649. DOI: 10.1108/03321641111152612.

[15] I. N. McCarthy, N. J. Adkins, Z. Aslam, A. M. Mullis, and R. F. Cochrane, "High speed imaging and fourier analysis of the melt plume during close coupled gas atomisation," EN, *Powder Metallurgy*, vol. 52, no. 3, pp. 205–212, Sep. 2009, ISSN: 0032-5899. DOI: 10.1179/174329409X409549.

[16] T. Zhao, C. Chen, X. Liu, and J. Hao, "Effect of gas mach number on the flow field of close-coupled gas atomization, particle size and cooling rate of as-atomized powder: Simulation and experiment," *Advanced Powder Technology*, vol. 34, no. 5, p. 104 007, May 2023, ISSN: 0921-8831. DOI: 10.1016/j.apt.2023.104007.

[17] M. L. Grasso and B. M. Colosimo, "Monitoring of Metal Additive Manufacturing Processes via In-Situ Machine Sensorization," eng, in *Proceedings of the IMEKO TC10 Workshop on New Perspectives in Measurements, Tools and Techniques for systems reliability, maintainability and safety*, 2016, ISBN: 978-92-990073-9-6. [Online]. Available: https://re.public.polimi.it/handle/11311/1016905.2.

[18] V. Uralde, F. Veiga, A. Suarez, A. Lopez, I. Goenaga, and T. Ballesteros, "Novel sensorized additive manufacturing-based enlighted tooling concepts for aeronautical parts," en, *Scientific Reports*, vol. 14, no. 1, p. 17 692, Jul. 2024, ISSN: 2045-2322. DOI: 10.1038/s41598-024-68786-w.

[19] F. Freeman, L. Chechik, B. Thomas, and I. Todd, "Calibrated closed-loop control to reduce the effect of geometry on mechanical behaviour in directed energy deposition," *Journal of Materials Processing Technology*, vol. 311, p. 117 823, Jan. 2023, ISSN: 0924-0136. DOI: 10.1016/j.jmatprotec.2022.117823.

[20] J.-F. Yao, Y. Yang, X.-C. Wang, and X.-P. Zhang, "Systematic review of digital twin technology and applications," *Visual Computing for Industry, Biomedicine, and Art*, vol. 6, no. 1, p. 10, May 2023, ISSN: 2524-4442. DOI: 10.1186/s42492-023-00137-4.

[21] S. V. Roth, "A deep look into the spray coating process in real-time—the crucial role of x-rays," en, *Journal of Physics: Condensed Matter*, vol. 28, no. 40, p. 403 003, Aug. 2016, ISSN: 0953-8984. DOI: 10.1088/0953-8984/28/40/403003.

[22] D. E. Lawrynowicz and E. J. Lavernia, "Sensors and techniques used to monitor processing parameters during spray atomization and deposition," en, *Journal of Materials Science*, vol. 30, no. 5, pp. 1125–1138, Mar. 1995, ISSN: 1573-4803. DOI: 10.1007/BF00356110.

[23] G. Chen, Q. Zhou, S. Y. Zhao, J. O. Yin, P. Tan, Z. F. Li, Y. Ge, J. Wang, and H. P. Tang, "A pore morphological study of gas-atomized Ti-6Al-4V powders by scanning electron microscopy and synchrotron X-ray computed tomography," *Powder Technology*, vol. 330, pp. 425–430, May 2018, ISSN: 0032-5910. DOI: 10.1016/j.powtec.2018.02.053.

[24] Mistras, *Wideband Differential Acoustic-Emission Sensor Datasasheet*, en, 2025. [Online]. Available: https://www.physicalacoustics.com/by-product/sensors/WD-100-900-kHz-Wideband-Differential-AE-Sensor.

[25] Polytec, *VibroGo OFV-5000 Datasheet*, en, 2025. [Online]. Available: https://www.polytecstore.fr/polytec_images/documents/oms/om_ds_vibrogo_e_52039.pdf.

[26] H. H. Nassif, M. Gindy, and J. Davis, "Comparison of laser doppler vibrometer with contact sensors for monitoring bridge deflection and vibration," *NDT & E International*, Structural Faults and Repair, vol. 38, no. 3, pp. 213–218, Apr. 2005, ISSN: 0963-8695. DOI: 10.1016/j.ndteint.2004.06.012.

[27] P. AI. "EVK4 - HD," Accessed: Jul. 23, 2025. [Online]. Available: https://docs.prophesee.ai/stable/hw/evk/evk4.html.

[28] G. Gallego, T. Delbruck, G. Orchard, C. Bartolozzi, B. Taba, A. Censi, S. Leutenegger, A. Davison, J. Conradt, K. Daniilidis, and D. Scaramuzza, "Event-based vision: A survey," *IEEE Trans. Pattern Anal. Mach. Intell.*, vol. 44, no. 1, pp. 154–180, Jan. 1, 2022, ISSN: 0162-8828, 2160-9292, 1939-3539. DOI: 10.1109/TPAMI.2020.3008413.

[29] D. Miller and E. Canzini, *Analysis of sensing modalities for electrode-induction gas atomization of metal powders*, Jul. 2025. DOI: 10.15131/shef.data.c.7911689.

[30] S. Mállat, *A Wavelet Tour of Signal Processing*. Springer, 2008, ISBN: 978-0-12-374370-1. DOI: 10.1016/B978-0-12-374370-1.X0001-8.

[31] W. Alexander and C. Williams, *Digital Signal Processing: Principles, Algorithms and System Design*. Elsevier, 2017, ISBN: 978-0-12-804547-3.

[32] K. P. Murphy, *Probabilistic Machine Learning: An introduction*. MIT Press, 2022. [Online]. Available: http://probml.github.io/book1.

[33] "Scipy 1.0: Fundamental algorithms for scientific computing in python," *Nature Methods*, vol. 17, pp. 261–272, 2020. DOI: 10.1038/s41592-019-0686-2. Accessed: May 19, 2025.

[34] R. Benosman, C. Clercq, X. Lagorce, S.-H. Ieng, and C. Bartolozzi, "Event-based visual flow," *IEEE Transactions on Neural Networks and Learning Systems*, vol. 25, no. 2, pp. 407–417, Feb. 2014, ISSN: 2162-2388. DOI: 10.1109/TNNLS.2013.2273537.

[35] V. Vasco, A. Glover, and C. Bartolozzi, "Fast event-based harris corner detection exploiting the advantages of event-driven cameras," in *2016 IEEE/RSJ International Conference on Intelligent Robots and Systems (IROS)*, Oct. 2016, pp. 4144–4149. DOI: 10.1109/IROS.2016.7759610.

[36] S. Shiba, Y. Aoki, and G. Gallego, "Fast Event-based Optical Flow Estimation by Triplet Matching," *IEEE Signal Processing Letters*, vol. 29, pp. 2712–2716, 2022, ISSN: 1070-9908, 1558-2361. DOI: 10.1109/LSP.2023.3234800.

[37] R. Ranade, C. Hill, and J. Pathak, "DiscretizationNet: A machine-learning based solver for Navier–Stokes equations using finite volume discretization," *Computer Methods in Applied Mechanics and Engineering*, vol. 378, p. 113 722, May 2021, ISSN: 0045-7825. DOI: 10.1016/j.cma.2021.113722.

[38] L. Regenwetter, A. H. Nobari, and F. Ahmed, "Deep Generative Models in Engineering Design: A Review," *Journal of Mechanical Design*, vol. 144, no. 071704, Mar. 2022, ISSN: 1050-0472. DOI: 10.1115/1.4053859. [Online]. Available: https://doi.org/10.1115/1.4053859.

[39] J. E. Naranjo, M. M. Llumiquinga, W. D. Vaca, and C. X. Espin, "Generative AI vs. Traditional Databases: Insights from Industrial Engineering Applications," en, *Publications*, vol. 13, no. 2, p. 14, 2025, ISSN: 2304-6775. DOI: 10.3390/publications13020014.

Dr. Ethan Canzini is a Research Associate in the School of Manufacturing, Aerospace & Civil Engineering at the University of Sheffield, where he specialises in systems and control engineering. He obtained a Masters of Engineering in aerospace engineering with a double minor in control theory and robotics and a PhD where his work focused on combining formal methods in control with machine learning approaches in the fields of robotics, space systems, metamaterials and process control.

He is the co-lead of the Robotics & Autonomous Manufacturing Systems Lab (RAMS Lab), and has supervised multiple projects relating to autonomous systems in manufacturing. Before joining academia, he worked in the semiconductor and aerospace industries.

David Miller is a PhD student in the School of Manufacturing, Aerospace & Civil Engineering where he specialises in data science and image processing. He obtained a Masters in Mechatronics & Robotics, and is currently conducting PhD research focusing on decentralized systems for sharing product information.

Dr. Divya Tiwari is a Research Fellow working in the Digitisation Laboratory for Manufacturing at the University of Sheffield. Her work focuses on sensors and simulation for manufacturing and re-manufacturing processes. Divya has published extensively within the field of digital manufacturing in areas such as simulation, sensorisation and in-process monitoring of manufacturing processes. She gained experience working as a lead researcher in several high-value grants, such as the Future Electrical Machines Manufacturing Hub and the platform grants. She has supervised several BEng and MEng students and supported many PhD students.

She was awarded the Daphne Jackson and Royal Academy of Engineering Fellowship in 2013 for the development of novel photonic sensors for industrial applications. Divya holds a PhD awarded by Cranfield University. Before joining academia, Divya worked in the electronics industry on aerospace and automotive applications in the UK.

Dr. Windo Hutabarat is a Research Associate in the School of Mechanical, Aerospace & Civil Engineering at the University of Sheffield. His concept of applying affordable machine vision innovations from the gaming sector into manufacturing and services was developed into multiple collaborative research projects with industry. He currently works on the digitalisation of manual aerostructure assembly processes in the aerospace sector, particularly on the application of deep learning to improve factory productivity.

Prof. Allan Matthews is Professor of Surface Engineering and Tribology in the Department of Materials at the University of Manchester. He is a member of the Henry Royce Institute and Director of the EPSRC Network Plus in Digital Surface Manufacturing.

Prof. Ashutosh Tiwari is Deputy Vice-President for Innovation at the University of Sheffield and holds the prestigious RAEng/Airbus Research Chair. He is internationally renowned for research in digital manufacturing and works in partnership with industry to develop new techniques and solutions for digitalisation in manufacturing operations.

He has a strong track record of leading research and innovation projects across technology readiness levels, and serves on the EPSRC Strategic Advisory Team for Manufacturing and the Circular Economy. He is Deputy Director of the EPSRC Future Electrical Machines Manufacturing Hub, Sheffield Lead of the Made Smarter Research Centre for Connected Factories, and was awarded an EPSRC High-Value Manufacturing Catapult Fellowship.